LBNL-40365

ERNEST ORLANDO LAWRENCE
BERKELEY NATIONAL LABORATORY

Comparison of Scale Analysis and Numerical Simulation for Saturated Zone Convective Mixing Processes

Curtis M. Oldenburg

Earth Sciences Division

June 1998

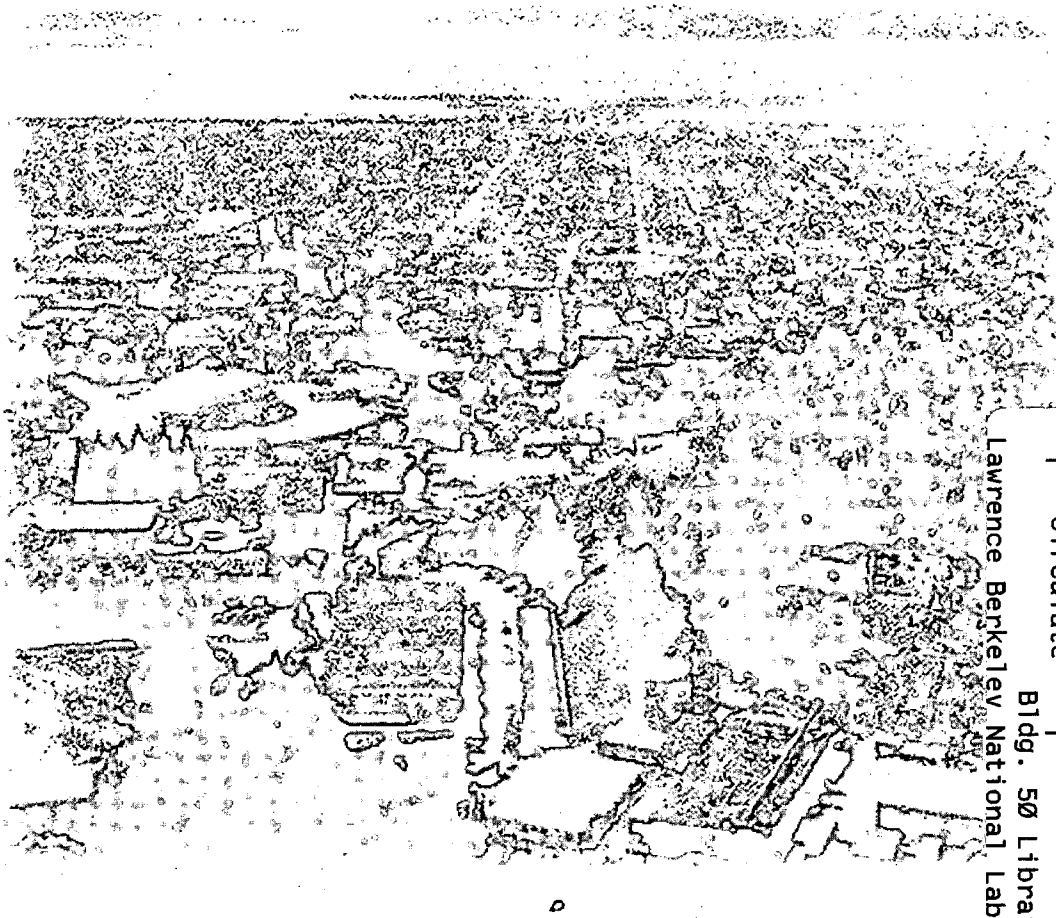

DISCLAIMER

LBNL- 40365

Comparison of Scale Analysis and Numerical Simulation for Saturated Zone Convective Mixing Processes

Curtis M. Oldenburg

Earth Sciences Division
Ernest Orlando Lawrence Berkeley National Laboratory
Berkeley CA 94720

1 June 1998

This work was supported by the Director, Office of Civilian Radioactive Waste Management, U.S. Department of Energy, through Memorandum Purchase Order EA9013MC5X between TRW Environmental Safety Systems Incorporated and Ernest Orlando Lawrence Berkeley National Laboratory, under Contract No. DEAC03-76SF00098.

Abstract

Scale analysis can be used to predict a variety of quantities arising from natural systems where processes are described by partial differential equations. For example, scale analysis can be applied to estimate the effectiveness of convective mixing on the dilution of contaminants in groundwater. Scale analysis involves substituting simple quotients for partial derivatives and identifying and equating the dominant terms in an order-of-magnitude sense. For free convection due to sidewall heating of saturated porous media, scale analysis shows that vertical convective velocity in the thermal boundary layer region is proportional to the Rayleigh number, horizontal convective velocity is proportional to the square root of the Rayleigh number, and thermal boundary layer thickness is proportional to the inverse square root of the Rayleigh number. These scale analysis estimates are corroborated by numerical simulations of an idealized system. A scale analysis estimate of mixing time for a tracer mixing by hydrodynamic dispersion in a convection cell also agrees well with numerical simulation for two different Rayleigh numbers. Scale analysis for the heating-from-below scenario produces estimates of maximum velocity one-half as large as the sidewall case. At small values of the Rayleigh number, this estimate is confirmed by numerical simulation. For larger Rayleigh numbers, simulation results suggest maximum velocities are similar to the sidewall heating scenario. In general, agreement between scale analysis estimates and numerical simulation results serves to validate the method of scale analysis.

Introduction

Scale analysis can be used to predict a variety of quantities arising from natural systems where processes are described by partial differential equations (PDEs). The method of scale analysis has been well described for heat and mass transfer in viscous fluids by Bejan (1985) and by Trevisan and Bejan (1985) for porous media. Scale analysis has been applied to magmatic systems with comparison to numerical simulation for validation (Spera et al., 1989). The essence of scale analysis is the replacement of partial derivatives in the PDEs with simple quotient terms, and the identification of the dominant terms in each PDE. The order-of-magnitude equivalence of the dominant terms allows one to solve for various quantities of interest such as velocity, length scales, and time scales as functions of problem parameters.

The power of scale analysis is that it can be used to obtain order-of-magnitude estimates of system behavior with pencil and paper. Although numerical and analytical methods provide essentially correct solutions to PDEs, scale analysis is a useful technique for preliminary studies to understand processes in an order-of-magnitude sense. However, because of the simplicity of scale analysis relative to analytical and numerical methods of solving PDEs, scale analysis predictions are often looked upon with suspicion while numerical simulation results are given greater credibility.

The main purpose of this report is to validate scale analysis predictions by showing their agreement to numerical simulation results for an idealized system that considers the mixing of a passive tracer. Whereas prior work on scale analysis of convective processes has focussed on heat transfer, the main motivation for the present study is the prediction of the time scales for convective mixing of groundwater contaminants in the saturated zone where aquifers are subject to destabilizing temperature gradients. The term convective mixing as used here refers to mixing by hydrodynamic dispersion in a flow field driven by natural convection. When destabilizing temperature

gradients are lateral as in sidewall heating, or vertical as in the heating-from-below scenario, the potential for natural convection arises. The strength of the resulting convective flow is a function of parameters such as the permeability and relevant length scale. In the study presented here, comparisons of scale analysis and numerical simulation will show that appropriately applied scale analysis gives useful order-of-magnitude estimates of quantities of interest for natural convection in saturated porous media systems. Although the presentation centers on particular configurations of natural convection, the methods are in fact general and can be applied to a wide variety of systems described by PDEs.

Scale Analysis

Scale analysis can provide order-of-magnitude estimates for fundamental quantities of interest such as velocities, length scales, and time scales from PDEs. Here application of the method to a free convection problem in saturated porous media will be presented. The system (Fig. 1) consists of a two-dimensional square region of saturated porous media in which the left-hand sidewall is held at a constant temperature of 60 °C and the the right-hand sidewall is held at 50 °C. The top and bottom boundaries are closed to heat and mass transfer.

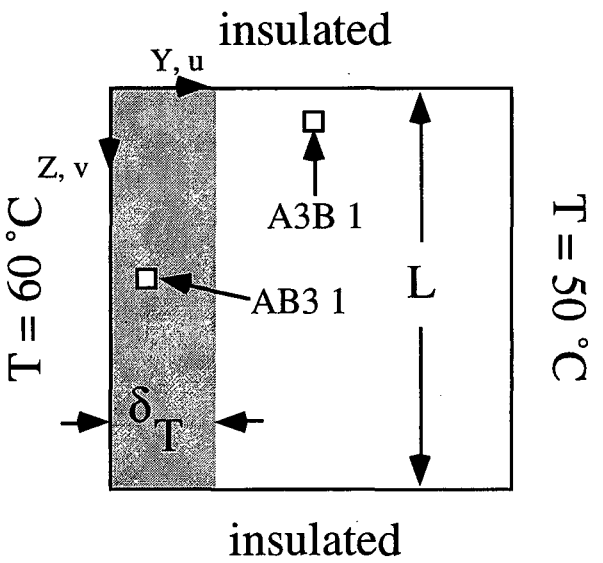

Fig. 1. Domain and boundary conditions for sidewall free convection problem. The shaded region on the left-hand side is the region in which the scale analysis is carried out. The locations of gridblocks AB3 1 and A3B 1 are shown.

The first step in scale analysis is to write down the PDEs that govern the processes of interest. The steady-state PDEs governing saturated porous media convection in two dimensions with the Boussinesq approximation are:

continuity: $$\frac{\partial u}{\partial y}+\frac{\partial v}{\partial z}=0 \qquad (1)$$

Y-Darcy velocity: $$u = -\frac{k}{\mu}\left(\frac{\partial P}{\partial y}\right) \qquad (2a)$$

Z-Darcy velocity: $$v = -\frac{k}{\mu}\left(\frac{\partial P}{\partial z}+\rho g\right) \qquad (2b)$$

energy: $$u\frac{\partial T}{\partial y}+v\frac{\partial T}{\partial z}=\frac{K}{\rho C_p}\left(\frac{\partial^2 T}{\partial y^2}+\frac{\partial^2 T}{\partial z^2}\right) \qquad (3)$$

species: $$u\frac{\partial X^{\kappa}}{\partial y}+v\frac{\partial X^{\kappa}}{\partial z}=\overline{\mathbf{D}}^{\kappa}\left(\frac{\partial^2 X^{\kappa}}{\partial y^2}+\frac{\partial^2 X^{\kappa}}{\partial z^2}\right) \qquad (4).$$

(See nomenclature for definition of symbols). Although here the focus is on pure thermal convection rather than double-diffusive convection, the species conservation equation (Eq. 4) is included for completeness since mixing of solute species will be considered. The driving force in free convection is buoyancy, specified by the last term in Eq. 2b, where density can be represented by a simple function of temperature and concentration given by

$$\rho=\rho_0\left(1-\alpha(T-T_0)+\beta\left(X^{\kappa}-X_0^{\kappa}\right)\right) \qquad (5)$$

where

$$\alpha=-\frac{1}{\rho_0}\left(\frac{\partial\rho}{\partial T}\right) \qquad (6)$$

and

$$\beta=\frac{1}{\rho_0}\left(\frac{\partial\rho}{\partial X^{\kappa}}\right) \qquad (7).$$

The dispersion tensor of Eq. 4 is given in terms of molecular diffusivity and transverse and longitudinal dispersivities after (de Marsily, 1986) as

$$\overline{\mathbf{D}}^{\kappa} = D_T^{\kappa}\,\overline{\mathbf{I}} + \frac{D_L^{\kappa} - D_T^{\kappa}}{u^2}\,\mathbf{u}\,\mathbf{u} \tag{8}$$

where

$$D_T^{\kappa} = \phi\,\tau o\,d^{\kappa} + \alpha_T u \tag{9}$$

$$D_L^{\kappa} = \phi\,\tau o\,d^{\kappa} + \alpha_L u \tag{10}.$$

The second step in scale analysis is the wise choice of a subregion in which the scale analysis will be performed. A useful subregion for the present sidewall heating problem is shown shaded in Fig. 1. The characteristic height of the subregion is L, and its width is δ_T.

The partial derivatives in the PDEs of Eqs. 1-4 can be converted into simple quotients applicable to the subregion in Fig. 1. Specifically, from Eq. 1, one obtains

$$\frac{u}{\delta_T} \sim \frac{v}{L} \tag{11}.$$

Because we consider natural convection as the driving force for the flow, in Eq. 2b it is assumed that upward-directed buoyancy drives the flow making the pressure gradient negligible relative to the buoyancy term. Substituting Eq. 5 for the fluid density in Eq. 2b and assuming negligible solutal buoyancy effects results in the relation:

$$v \sim \frac{k}{\mu}\rho\,\alpha\,\Delta T\,g \tag{12}.$$

The energy equation (Eq. 3) applied in the subregion shows that vertical advection is balanced by horizontal conduction:

$$v \frac{\Delta T}{L} \sim \frac{K}{\rho C_p} \frac{\Delta T}{\delta_T^2} \qquad (13).$$

where the quotient $K/\rho\, C_p$ represents the thermal diffusivity of the aqueous phase. Introducing the fundamental parameter of free convection, the Rayleigh number (Ra),

$$Ra = \frac{\rho\, \alpha\, \Delta T\, g\, k\, L}{\frac{K}{\rho\, C_p} \mu} \qquad (14)$$

and substituting Eq. 14 into Eq. 12, one obtains

$$v \sim \frac{K}{\rho\, C_p\, L} Ra \qquad (15).$$

This is the first useful estimate of the scale analysis and states that the order of magnitude of the vertical Darcy velocity (v) is directly proportional to Ra and thermal conductivity, inversely proportional to L , and that its order of magnitude is given by Eq. 15.

Combining Eq. 13 with Eq. 15 results in an estimate for the thermal boundary layer thickness,

$$\delta_T \sim \left(\frac{K}{\rho\, C_p} \frac{L}{v}\right)^{1/2} \sim \left(\frac{K}{\rho\, C_p} \frac{L^2}{\frac{K}{\rho\, C_p} Ra}\right)^{1/2} \sim L\, Ra^{-1/2} \qquad (16).$$

Combining Eq. 11 with Eqs. 15 and 16 gives an estimate for the horizontal Darcy velocity, u, in the subregion,

$$u \sim \frac{K}{\rho\, C_p\, L} Ra^{1/2} \qquad (17).$$

Eqs. 15, 16, and 17 represent order of magnitude estimates for the velocities and boundary layer thicknesses for the subregion of the free convection problem.

Comparison to Numerical Simulation Results

In this section, the predictions of the scale analysis (Eqs. 15, 16, and 17) are compared with steady-state numerical solutions from TOUGH2 (Pruess, 1987; 1991) of free convection for the system shown in Fig. 1. The equations solved in TOUGH2 consider non-isothermal physical properties of water as well as a full, i.e., non-boussinesq, treatment of density. Nevertheless, it will be shown that the order-of-magnitude estimates agree well. Parameters for the problem are presented in Table 1. The grid is 200 m by 200 m and consists of 20 x 20 gridblocks 10 m on a side with narrow rows and columns of gridblocks along the boundaries for implementing various boundary conditions.

Shown in Figs. 2 and 3 are steady-state results for the velocity and temperature fields for a case with Ra = 103, and Ra = 1030, respectively. The flow is clockwise up the hot left-hand side boundary and down the colder right-hand side. The largest pore velocities in each figure are given by the number shown above the temperature scale, specifically 2 x 10^{-7} m s^{-1} (6 m yr^{-1}), and 2 x 10^{-6} m s^{-1} (60 m yr^{-1}), respectively. These pore velocities will be converted to Darcy velocities for comparison with the scale estimates of Eqs. 15 and 17. Note the narrower thermal boundary layer for the Ra = 1030 case relative to the Ra = 103 case.

Table 1. Parameters for pure thermal convection.

Parameter	Value
porosity	0.2
permeability (case I. $Ra = 103$)	1×10^{-12} m^2
permeability (case II. $Ra = 1030$)	1×10^{-11} m^2
thermal conductivity of the formation	1.8 J m^{-1} s^{-1} °C^{-1}
density of the solid grains	2650 kg m^{-3}
heat capacity of the solid grains	1000 J kg^{-1} °C^{-1}
height	200 m
width	200 m
left-hand sidewall temperature	60 °C
right-hand sidewall temperature	50 °C
gravitational acceleration	9.806 m s^{-2}
viscosity (T = 50 °C)	0.55×10^{-3} Pa s
density (T = 50 °C)	988 kg m^{-3}
thermal expansivity (T = 55 °C)	4.55×10^{-4} °C^{-1}
thermal diffusivity ($K/(\rho C_p)$ at T = 55 °C)	1.57×10^{-7} m^2 s^{-1}

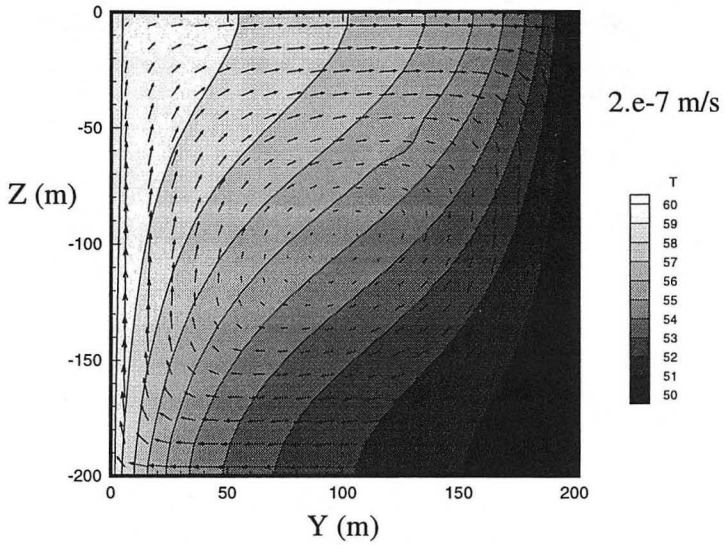

Fig. 2. Temperature and pore velocity field for the steady-state sidewall heating pure thermal convection problem with Ra = 103. The magnitude of the largest pore velocity vector is given by the number above the temperature scale, specifically 2 x 10^{-7} m s^{-1} (6 m yr^{-1})

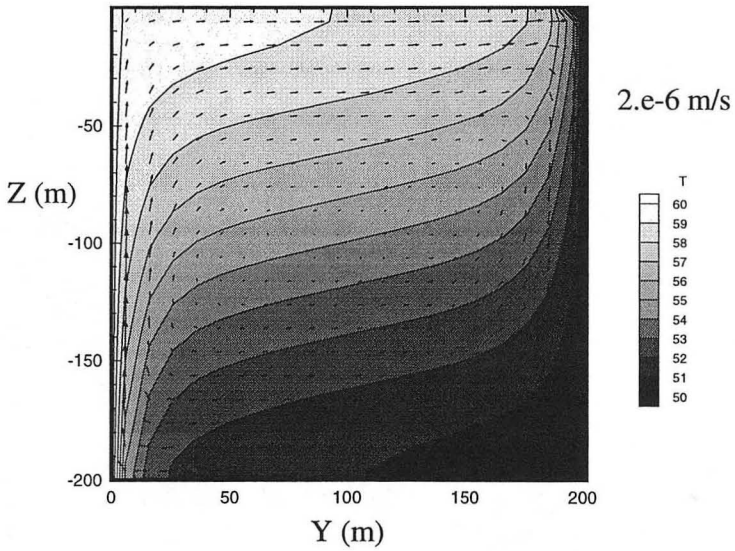

Fig. 3. Temperature and pore velocity field for the steady-state sidewall heating pure thermal convection problem with Ra = 1030.

Table 2 presents a comparison of scale analysis predictions with numerical simulation results. The numerical results for characteristic vertical and horizontal velocity are taken as the Darcy velocity between gridblock AB3 1 and AC3 1 (horizontal flow), and AB3 1 and AB4 1 (vertical flow), where the approximate location of AB3 1 is shown in Fig. 1. The thermal boundary layer thickness is arbitrarily defined here as the thickness at Z = -100 m of the region that is hotter than 58 °C. As shown in Table 2, the numerical simulation results agree in an order-of-magnitude sense with the scale analysis and serve to validate the scale analysis.

Table 2. Comparison of scales derived from scale analysis and numerical simulation.

Ra	quantity	scale analysis	numerical simulation
103	v	8 x 10^{-8} m s^{-1}	2.4 x 10^{-8} m s^{-1}
	u	8 x 10^{-9} m s^{-1}	3.2 x 10^{-9} m s^{-1}
	δ_T	20 m	30 m
1030	v	8 x 10^{-7} m s^{-1}	1.3 x 10^{-7} m s^{-1}
	u	2.5 x 10^{-8} m s^{-1}	2.4 x 10^{-8} m s^{-1}
	δ_T	6 m	10 m

Mixing Time

Scale Analysis

In this section, an order-of-magnitude estimate for the mixing time of a solute is made for the thermal convection flow problem. With the assumption of a reference frame moving with the Darcy velocity (v), the one-dimensional transient species conservation equation, where the coordinate s is perpendicular to the streamlines, can be written:

$$\frac{\partial X^{\kappa}}{\partial t} = \left(d^{\kappa} + \alpha_T v\right)\frac{\partial^2 X^{\kappa}}{\partial s^2} \qquad (18).$$

A scale analysis of Eq. 18 gives

$$\frac{\Delta X^{\kappa}}{\tau} \sim \left(d^{\kappa} + \alpha_T v\right) \frac{\Delta X^{\kappa}}{\delta^2} \tag{19}$$

which simplifies to

$$\tau \sim \frac{\delta^2}{\left(d^{\kappa} + \alpha_T v\right)} \tag{20}$$

where τ is the characteristic dispersive time scale and δ is the characteristic dispersive length scale. For typical solute species, molecular diffusivity in the aqueous phase is less than approximately 1 x 10^{-8} m^2 s^{-1}. For the system considered here with Ra = 103, the convective velocity is approximately 8 x 10^{-8} m s^{-1}, thus making molecular diffusion negligible relative to dispersion for large-scale flows in nature. This results in the following relation between dispersive mixing time and convective Darcy velocity:

$$\tau \sim \frac{\delta^2}{\alpha_T v} \tag{21}.$$

To derive a mixing time due to hydrodynamic dispersion, it is assumed that the system is mixed when the dispersive length scale is one-half of the system dimension (L/2), or

$$\tau_{mix} \sim \frac{L^2}{4\alpha_T v} \tag{22}.$$

Substituting Eq. 15 for v into Eq. 22 provides an estimate of the mixing time in terms of Ra:

$$\tau_{mix} \sim \frac{L^3}{4\alpha_T \frac{K}{\rho C_p} Ra} \tag{23}.$$

For the base case scenario with Ra = 103, L = 200 m, and α_T = 20 m, and other parameters as shown in Table 1, the mixing time is predicted to be of order 200 yrs.

Numerical Simulation

To compare the estimate of Eq. 23 with numerical simulation results, it is necessary to use T2DM, the two-dimensional dispersion module for TOUGH2 (Oldenburg and Pruess, 1993), to calculate mixing of a passive tracer component due to natural convection with hydrodynamic dispersion. In the problem, tracer is injected for 100 days into gridblock A3B 1 (Fig. 1). The tracer may be referred to as a brine component here but is in fact a tracer since all of the brine properties are identical to those of water. The flow field is at steady state throughout the convective mixing process. Parameters for the problem are identical to those in Table 1 except for the addition of non-zero dispersivities. To illustrate the strong effects of hydrodynamic dispersion on convective mixing, two cases are shown in this section: (1) convective mixing where hydrodynamic dispersion and molecular diffusion are zero; and (2) convective mixing with hydrodynamic dispersion where $\alpha_T = \alpha_L$ = 20 m.

For the case of zero dispersion, plots of the tracer mass fraction field and velocity are shown in Figs. 4–7 at t = 50, 100, 200, and 300 yrs. These plots show the general form of mixing in convection cells or recirculations. Note that the maximum concentration value is rescaled in each plot. Although the physical processes of dispersion and diffusion are set to zero, significant mixing still occurs due to dilution effects caused by flow in a variable velocity flow field (Oldenburg and Pruess, 1996) and by numerical dispersion. Nevertheless, tracer is slow to enter the center of the convection cell because convective velocities are small there and flow dilution and numerical dispersion are correspondingly small. Mixing processes are strongest in fast moving regions of the convection cell.

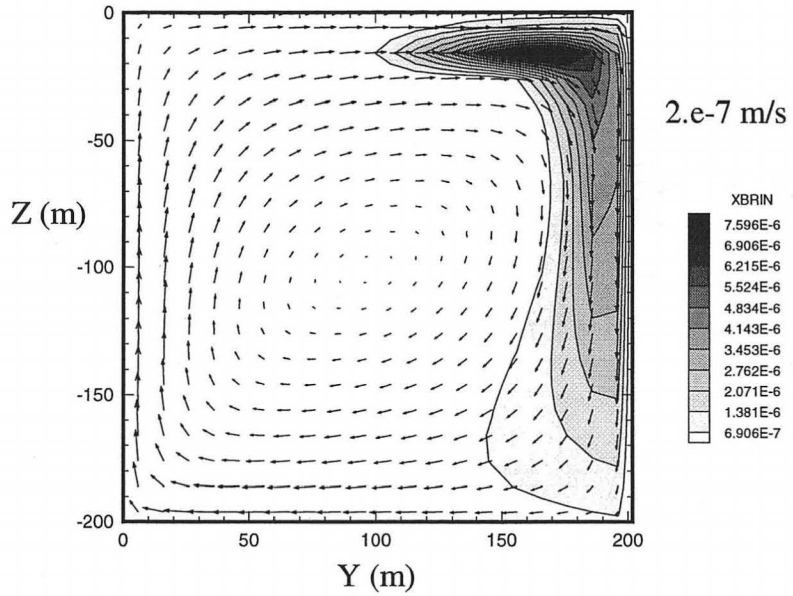

Fig. 4. Brine mass fraction and velocity field at t = 50 yrs for the sidewall heating pure thermal convective mixing problem with Ra = 103.

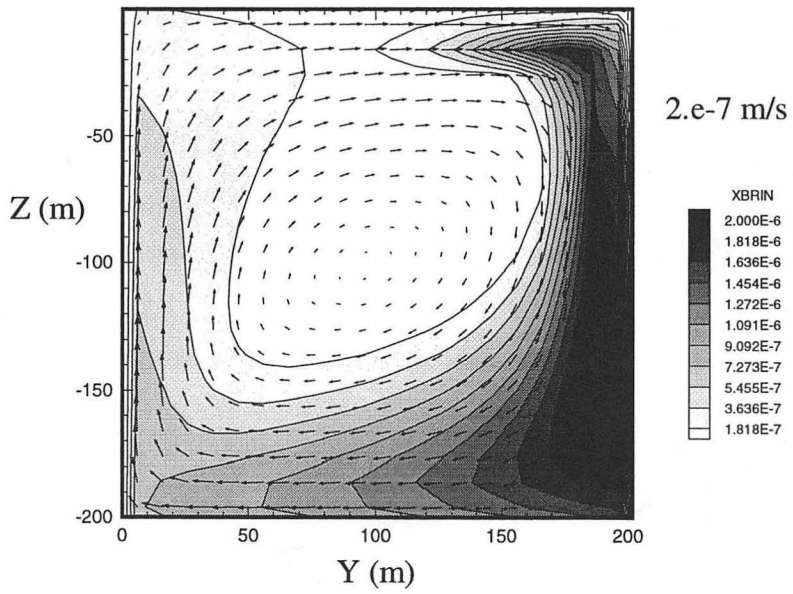

Fig. 5. Brine mass fraction and velocity field at t = 100 yrs for the sidewall heating pure thermal convective mixing problem with Ra = 103.

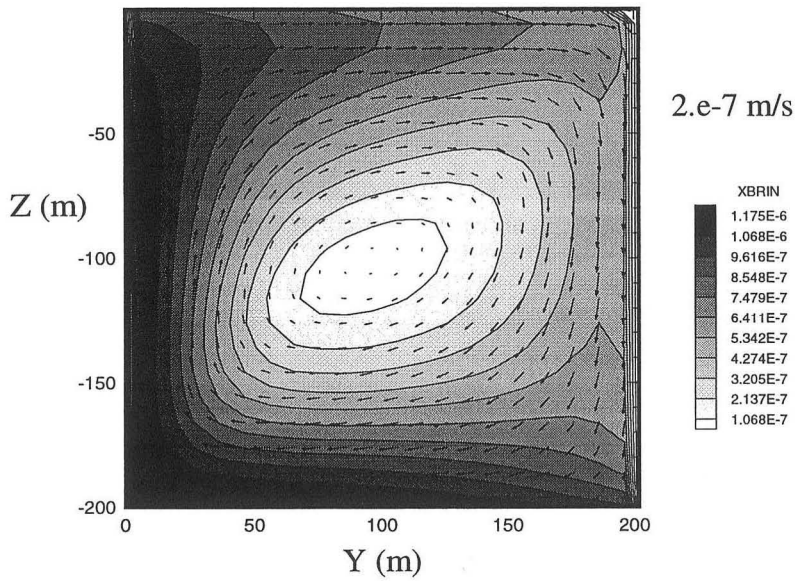

Fig. 6. Brine mass fraction and velocity field at $t = 200$ yrs for the sidewall heating pure thermal convective mixing problem with $Ra = 103$.

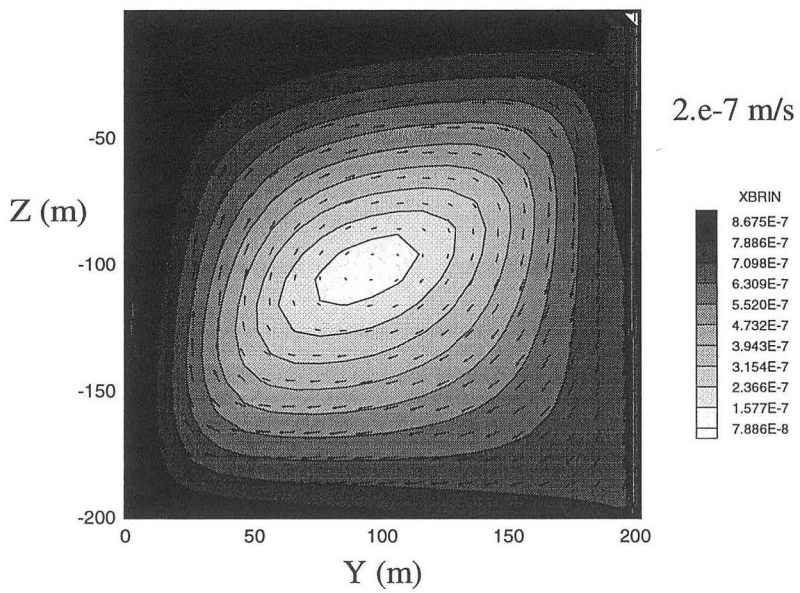

Fig. 7. Brine mass fraction and velocity field at $t = 300$ yrs for the sidewall heating pure thermal convective mixing problem with $Ra = 103$.

Shown in Figs. 8-10 are plots of the tracer mass fraction with velocity vectors superimposed at t = 100, 200, and 300 yrs for the case where $\alpha_T = \alpha_L = 20$ m. Direct comparison of Fig. 8 with Fig. 5 for mixing at t = 100 yrs for zero hydrodynamic dispersion and $\alpha_T = \alpha_L = 20$ m, respectively, shows that upstream dispersion has occurred. This is an undesirable artifact of the Fickian dispersion model (de Marsily, p. 242–243, 1986). As shown in Fig. 8, at t = 100 yrs there are still significant gradients in tracer mass fraction and, although displaced, the original mass injected is visible along the right-hand sidewall. At t = 200 yrs, gradients are greatly diminished. By t = 300 yrs, the system is almost totally mixed. Thus the mixing time estimate of 200 yrs from the scale analysis of Eq. 23 appears reasonable.

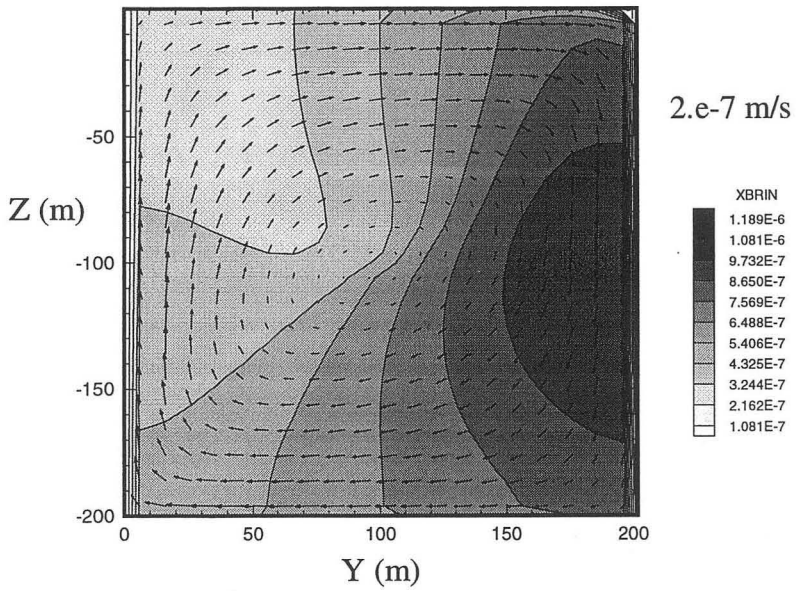

Fig. 8. Brine mass fraction and velocity field at t = 100 yrs for the sidewall heating pure thermal convective mixing problem with Ra = 103.

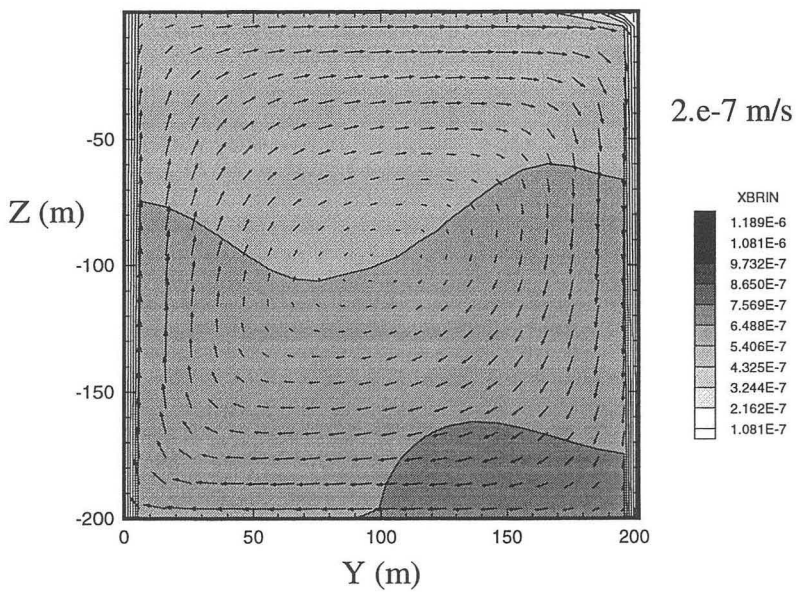

Fig. 9. Brine mass fraction and velocity field at t = 200 yrs for the sidewall heating pure thermal convective mixing problem with Ra = 103.

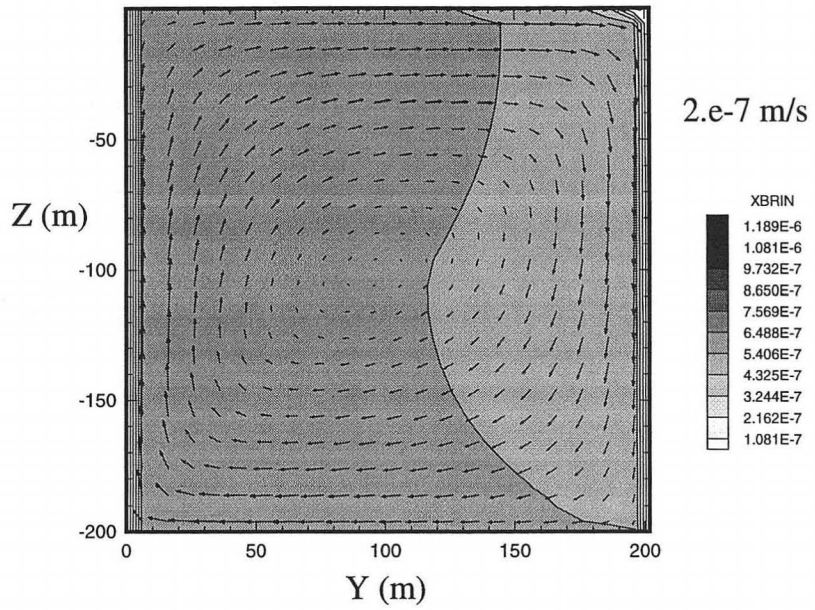

Fig. 10. Brine mass fraction and velocity field at t = 300 yrs for the sidewall heating pure thermal convective mixing problem with Ra = 103.

To check Eq. 23 further, results for a 10 times higher permeability (Ra = 1030) are presented in Figs. 11–13 at t = 10, 20, and 30 yrs. The temperature and flow field for this case were shown in Fig. 3. From Eq. 23, the predicted mixing time for this case is 20 yrs. Note first from Figs. 11–13 the overall similarity to the plots in Figs. 8–10 which are at 1/10 the Ra but at 10 times further out in time. This similarity lends credibility to the estimate of Eq. 23 since the time scale should be inversely proportional to Ra. By t =30 yrs for Ra = 1030, the tracer is essentially mixed.

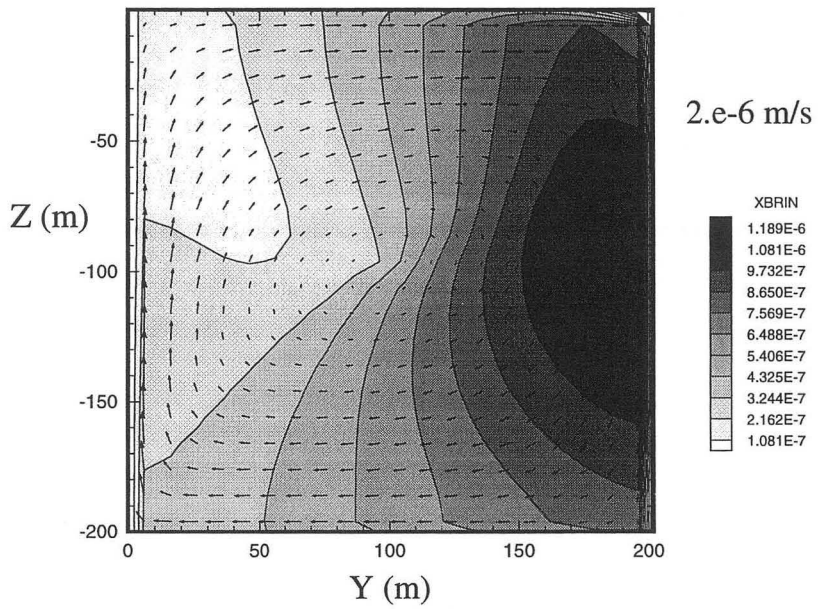

Fig. 11. Brine mass fraction and velocity field at t = 10 yrs for the sidewall heating pure thermal convective mixing problem with Ra = 1030.

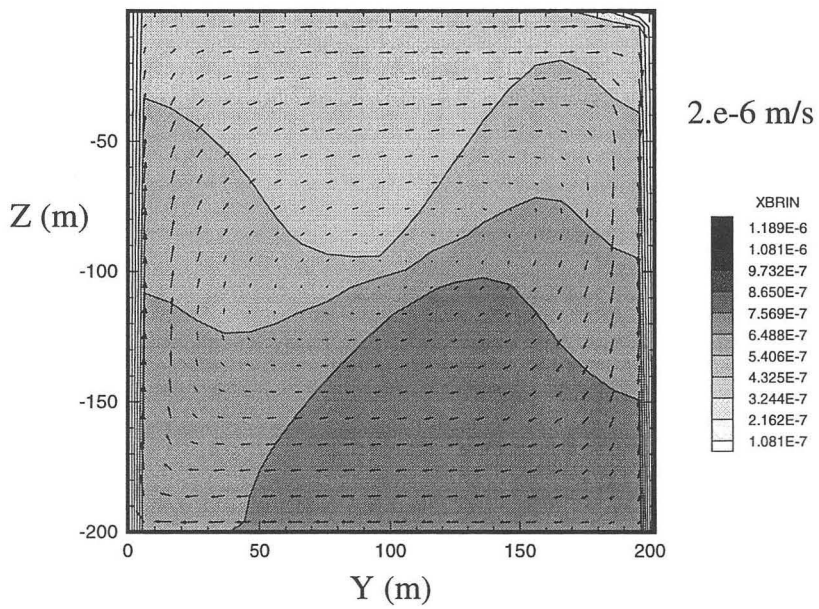

Fig. 12. Brine mass fraction and velocity field at t = 20 yrs for the sidewall heating pure thermal convective mixing problem with Ra = 1030.

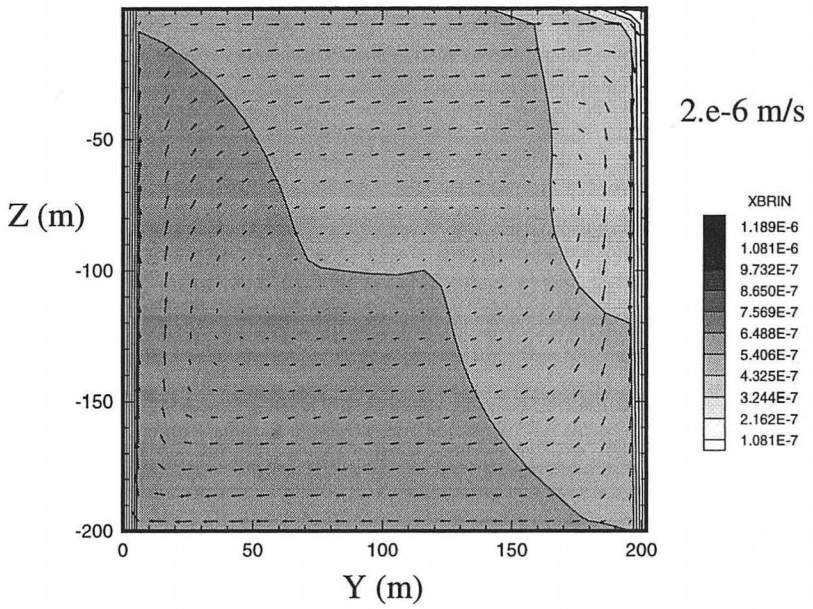

Fig. 13. Brine mass fraction and velocity field at t = 30 yrs for the sidewall heating pure thermal convective mixing problem with Ra = 1030.

Heating from Below

All of the above analysis has been for the case of sidewall heating. Heating from below is another common natural convection configuration. The domain and boundary conditions for the heated-from-below case are presented in Fig. 14. For the single roll, clockwise convection scenario, a plausible subregion for the scale analysis is along the bottom of the domain and has length L/2. The reason for the half-length is that in the single-roll convection scenario, buoyancy generated by heating produces upward motion only in one-half of the lower boundary region. In the other half, return flow from the cold upper parts of the domain causes downward motions. The subregion of length *L*/2 is shown shaded in Fig. 14.

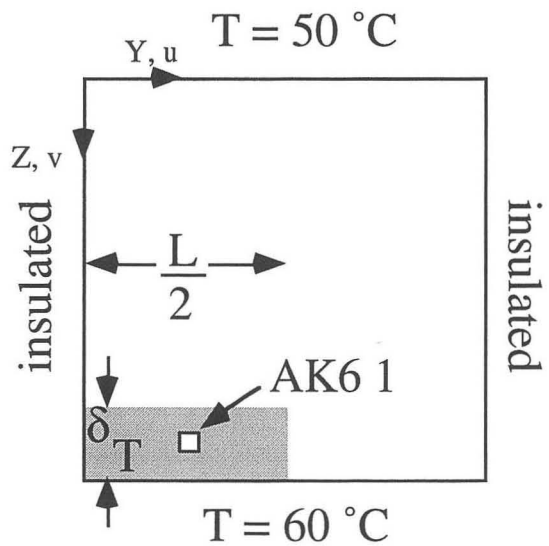

Fig. 14. Domain and boundary conditions for the heating-from-below thermal convection problem. The location of gridblock AK6 1 is shown for reference.

From the continuity, fluid velocity, and energy equations applied in the subregion, one obtains

$$\frac{2u}{L} \sim \frac{v}{\delta_T} \tag{24}$$

$$v \sim \frac{k}{\mu} \rho \alpha \Delta T g \frac{\delta_T}{L} \tag{25}$$

$$u \frac{\Delta T}{L} \sim \frac{1}{2} \frac{K}{\rho C_p} \frac{\Delta T}{\delta_T^2} \tag{26}.$$

In Eq. 25, the temperature difference available for buoyancy-driven vertical flow is assumed to be given by $\Delta T\ \delta_T/L$ in the subregion. Substituting Eq. 25 into Eq. 24 and introducing Ra (with characteristic length scale L as in Eq. 14) gives

$$u \sim \frac{1}{2} \frac{K}{\rho C_p L} Ra \tag{27}.$$

Substituting Eq. 27 into Eq. 26 results in the relation

$$\delta_T \sim \left(\frac{1}{2} \frac{K}{\rho C_p} \frac{L}{u}\right)^{1/2} \sim \left(\frac{1}{2} \frac{K}{\rho C_p} \frac{L^2}{\frac{1}{2} \frac{K}{\rho C_p} Ra}\right)^{1/2} \sim L\, Ra^{-1/2} \tag{28}.$$

Substituting Eq. 28 into Eq. 25 and using the definition of Ra results in the estimate for vertical velocity in the subregion

$$v \sim \frac{K}{\rho C_p L} Ra^{1/2} \tag{29}.$$

Thus the scale analysis estimates for δ_T and v (Eqs. 28 and 29, respectively) in the heating-from-below scenario are the same as for δ_T and u for the sidewall-heating scenario (Eqs. 16 and 17, respectively), while u in the heating-from-below scenario (Eq. 27) is $1/2v$ in the sidewall case (Eq. 15). The horizontal velocity, u, in the heating-from-

below scenario is the larger of the two velocity scales in the scale analysis domain. Therefore, u controls the overall vigor of convection in heating-from-below just as v controls vigor in sidewall heating.

Shown in Fig. 15 are the steady-state pore velocity and temperature field for the heating-from-below scenario with Ra = 103. As predicted, Darcy velocities are on the order of one-half the Darcy velocities for the sidewall-heating scenario. Presented in Table 3 is a summary of scale analysis predictions and numerical results where the horizontal Darcy velocity is from griblock AK5 1 to AK6 1 and the vertical Darcy velocity is from gridblock AJ6 1 to AK6 1. The thermal boundary layer thickness is defined as the thickness of the region hotter than 58 °C at Y = 46 m.

Table 3. Comparison of scales derived from scale analysis and numerical simulation.

Ra	quantity	scale analysis	numerical simulation
103	u	4×10^{-8} m s^{-1}	5.7×10^{-9} m s^{-1}
	v	8×10^{-9} m s^{-1}	2.2×10^{-9} m s^{-1}
	δ_T	20 m	24 m
1030	u	4×10^{-7} m s^{-1}	1.3×10^{-7} m s^{-1}
	v	2.5×10^{-8} m s^{-1}	8.6×10^{-10} m s^{-1}
	δ_T	6 m	10 m

The scale analysis and the numerical simulation both show that heating-from-below configurations are slightly less vigorous than sidewall-heating scenarios and convective mixing times will be correspondingly increased. Note that for the convection scenario of Fig. 15 with relatively small Ra, the isotherms are nearly conductive and yet convective mixing will occur. Substituting u from Eq. 27 for v in Eq. 22 gives an estimated mixing time on the order of twice as long for heating from below as for

sidewall heating at the same Ra. Thus mixing times for α_T = 20 m will be on the order of 400 yrs for Ra = 103.

The agreement between scale analysis and numerical simulation estimates of maximum velocity as shown in Table 3 are better for Ra = 1030 than for Ra = 103. This may be due to the fact that the heating-from-below scenario has a critical Rayleigh number of approximately 40 (Turcotte and Schubert, 1984, p. 405). Since the scale analysis does not have any stability criterion information built into it, perhaps maximum velocities for systems with a critical Rayleigh number should not be expected to match well at smaller values of Ra, i.e., close to the critical value.

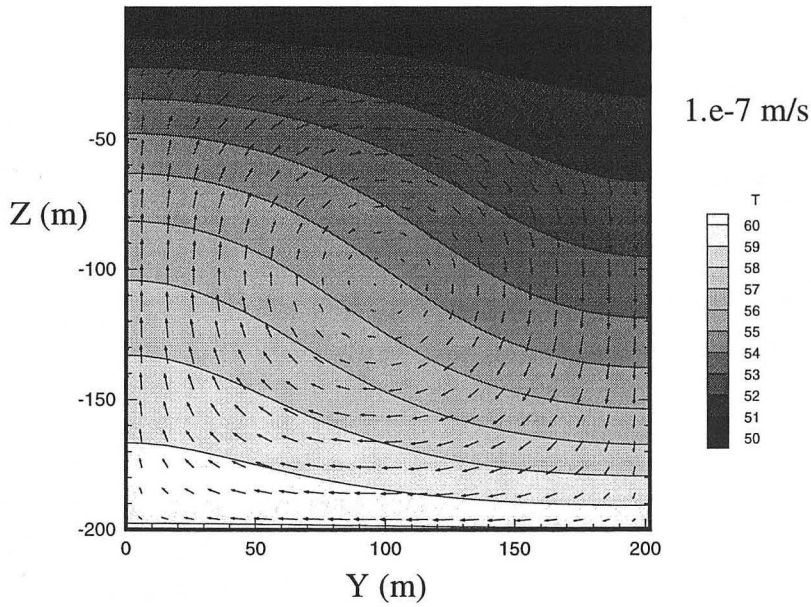

Fig. 15. Temperature and pore velocity field at steady state for the heating-from-below pure thermal convection problem with Ra = 103.

Summary and Conclusions

Comparisons of simple scale analysis and numerical simulation of idealized pure thermal convection in single-roll scenarios in saturated porous media show that scale analysis produces reliable order-of-magnitude estimates for fundamental aspects of convective flow and mixing. Summaries of scale analysis results are presented in Tables 4 and 5 for the sidewall-heating and heating-from-below scenarios.

Because *Ra* is linear with permeability (k), the permeability of an aquifer gives a good indication of the potential importance of mixing by natural convection, all other things being equal. In general, low permeability formations will produce slow convective velocities and long convective mixing times. In many aquifer systems, over the time scale of convective mixing, regional flow and the corresponding hydrodynamic dispersion may be more important mixing mechanisms. For high permeability formations and large temperature differences that produce instability, convective mixing can be an important mixing mechanism.

Table 4. Summary of scale analysis formulas for sidewall heating.

quantity	sidewall-heating
Vertical Darcy velocity	$v \sim \frac{K}{\rho C_p L} Ra$
Horizontal Darcy velocity	$u \sim \frac{K}{\rho C_p L} Ra^{1/2}$
Thermal boundary layer thickness	$\delta_T \sim L\, Ra^{-1/2}$
Convective mixing time	$\tau_{mix} \sim \frac{L^3}{4\alpha_T \frac{K}{\rho C_p} Ra}$

Table 5. Summary of scale analysis formulas for heating from below.

quantity	heating-from-below
Horizontal Darcy velocity	$u \sim \frac{1}{2} \frac{K}{\rho C_p L} Ra$
Vertical Darcy velocity	$v \sim \frac{K}{\rho C_p L} Ra^{1/2}$
Thermal boundary layer thickness	$\delta_T \sim L\, Ra^{-1/2}$
Convective mixing time	$\tau_{mix} \sim \frac{L^3}{2\alpha_T \frac{K}{\rho C_p} Ra}$

Nomenclature

d	molecular diffusivity, $m^2\ s^{-1}$.
C_p	heat capacity, $J\ kg^{-1}\ °C^{-1}$.
D_T	transversal hydrodynamic dispersion, $m^2\ s^{-1}$.
D_L	longitudinal hydrodynamic dispersion, $m^2\ s^{-1}$.
g	gravitational acceleration, $m\ s^{-2}$.
k	permeability, m^2.
K	thermal conductivity, $J\ m^{-1}\ °C^{-1}\ s^{-1}$.
L	length scale of the domain, m.
P	pressue, Pa.
Ra	Rayleigh number.
s	coordinate perpendicular to stream lines.
T	temperature, °C.
u,v	horizontal and vertical Darcy velocities, $m\ s^{-1}$.
y,z	horizontal and vertical coordinates, m.

Greek symbols

α	coefficient of thermal expansivity, $°C^{-1}$.
α_T	transversal dispersivity, m.

α_L	longitudinal dispersivity, m.
β	coefficient of solutal expansivity.
δ_T	thermal boundary layer thickness, m.
ϕ	porosity.
μ	viscosity, Pa s.
ρ	density, kg m^{-3}.
τ	time scale, s.
τo	tortuosity.

Supersripts and subscripts

κ	component
T	transversal
L	longitudinal
0	reference

Acknowledgments

This work was supported by the Director, Office of Civilian Radioactive Waste Management, U.S. Department of Energy, through Memorandum Purchase Order EA9013MC5X between TRW Environmental Safety Systems Incorporated and Ernest Orlando Lawrence Berkeley National Laboratory, under Contract No. DE-AC03-76SF00098. I thank Stefan Finsterle and Chao Shan for careful reviews.

References

Bejan, A., The method of scale analysis: Natural convection in fluids, in *Natural Convection: Fundamentals and Applications*, Kakaç, S., W. Aung, and R. Viskanta, Hemisphere, 1985.

de Marsily, G., *Quantitative Hydrogeology,* Academic Press, 440 pp., 1986.

Oldenburg, C.M. and K. Pruess, A two-dimensional dispersion module for the TOUGH2 simulator, *Lawrence Berkeley Laboratory Report, LBL- 32505*, 1993.

Oldenburg, C.M. and K. Pruess, Mixing with first-order decay in variable velocity porous media flow, *Transport in Porous Media*, *22*, 161–180, 1996.

Pruess, K., TOUGH User's Guide, Nuclear Regulatory Commission, Report NUREG/CR-4645, June 1987 (also *Lawrence Berkeley Laboratory Report, LBL-20700*, Berkeley, California, June 1987).

Pruess, K., TOUGH2 - A General Purpose Numerical Simulator for Multiphase Fluid and Heat Flow, *Lawrence Berkeley Laboratory Report, LBL-29400*, Berkeley, California, May 1991.

Spera, F.J., C.M. Oldenburg, and D.A. Yuen, Magma zonation: effects of chemical buoyancy and diffusion, *Geophys. Res. Lett., 16*(12), 1387–1390, 1989.

Trevisan, O.V., and A. Bejan, Natural convection with combined heat and mass transfer buoyancy effects in a porous medium, *Int. J. Heat Mass Transfer, 28*(8), 1597–1611, 1985.

Turcotte, D.L, and G. Schubert, Geodynamics Applications of Continuum Physics to Geological Problems, 450 pp., John Wiley & Sons, New York, 1982.

Ernest Orlando Lawrence Berkeley National Laboratory
One Cyclotron Road | Berkeley, California 94720

Prepared for the U.S. Department of Energy under Contract No. DE-AC03-76SF00098